Local Field Factors and Dielectric Properties of Liquid Benzene

Nazanin Davari,[†] Christopher D. Daub,[†] Per-Olof Åstrand,*,[†] and Mikael Unge[‡]

[†]Department of Chemistry, Norwegian University of Science and Technology (NTNU), NO-7491 Trondheim, Norway
[‡]ABB Corporate Research, SE-72178 Västerås, Sweden

S Supporting Information

ABSTRACT: Local electric field factors are calculated for liquid benzene by combining molecular dynamic simulations with a subsequent force-field model based on a combined charge-transfer and point-dipole interaction model for the local field factor. The local field factor is obtained as a linear response of the local field to an external electric field, and the response is calculated at frequencies through the first absorption maximum. It is found that the largest static local field factor is around 2.4, while it is around 6.4 at the absorption frequency. The linear susceptibility, the dielectric constant, and the first absorption maximum of liquid benzene are also studied. The electronic contribution to the dielectric constant is around 2.3 at zero frequency, in good agreement with the experimental value around 2.2, while it increases to 6.3 at the absorption frequency. The $\pi \to \pi^*$ excitation energy is around 6.0 eV, as compared to the gas-phase value of around 6.3 eV, while the experimental values are 6.5 and 6.9 eV for the liquid and gas phase, respectively, demonstrating that the gas-to-liquid shift is well-described.

$$\frac{\partial E_{H,y}^{loc}}{\partial E_y^{ext}} = 6$$

$$\frac{\partial E_{C,y}^{loc}}{\partial E_y^{ext}} = 2$$
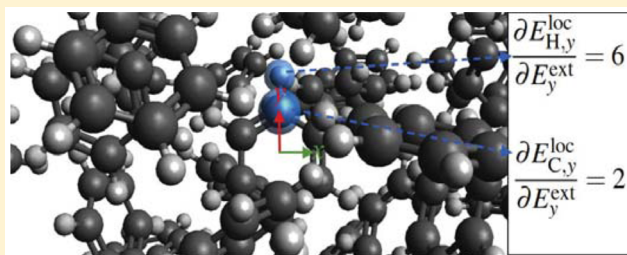
INTRODUCTION

In a molecular mechanics approach, the local electric field at an atom, $E_{I,\alpha}^{loc}$, is the sum of the external electric field, $E_{I,\alpha}^{ext}$, and the electric field of the permanent and induced multipole moments of the neighboring atoms, here restricted to atomic charges and atomic dipole moments,[1]

$$E_{I,\alpha}^{loc} = E_{I,\alpha}^{ext} + \sum_{J \neq I}^{N} \left(\frac{-R_{IJ,\alpha}}{\tilde{R}_{IJ}^3} q_J + \frac{3R_{IJ,\alpha}R_{IJ,\beta} - \delta_{\alpha\beta}\tilde{R}_{IJ}^2}{\tilde{R}_{IJ}^5} \mu_{J,\beta} \right) \tag{1}$$

where Greek subscripts α, β, and γ denote the Cartesian coordinates, and the Einstein summation convention is used for repeated subscripts. q_J is an atomic charge, and $\mu_{J,\beta}$ is an atomic dipole moment. To introduce a damping of the interatomic interactions at short distances, we extended the point-dipole interaction (PDI) model[2−6] by adding Gaussian charge distributions[7,8] similar to other approaches for describing short-range electrostatics.[9,10] In our model, $\tilde{R}_{IJ}$ is a scaled distance between atoms I and J,[7,11]

$$\tilde{R}_{IJ} = \sqrt{R_{IJ}^2 + \frac{\pi}{4\frac{\phi_I \phi_J}{\phi_I + \phi_J}}} \tag{2}$$

where ϕ_I is an atom-type parameter describing the width of a Gaussian charge distribution, and $R_{IJ,\alpha} = R_{I,\alpha} - R_{J,\alpha}$, where $R_{I,\alpha}$ is a component of the coordinate of atom I.

Local field effects at zero and optical frequencies are important in many applications. In surface-enhanced Raman scattering (SERS),[12−15] local field enhancement is observed in plasmonic nanoparticles showing very strong scattering of light due to the localized surface plasmon resonances.[16−18] In addition to metal nanoparticles, the plasmonic character of some aromatic molecules such as linear acenes also enhances the local field factor.[19] In resonance Raman and resonance hyper-Raman spectra,[20,21] the intermolecular vibronic coupling between solute molecules and neighboring solvent molecules causes enhanced local fields, a phenomenon called the molecular near-field effect.[22]

The local field at a molecule is caused by polarization of the surroundings, and it is a measure of the strength of the interaction between the solute and the solvent molecules and, thus, is used to determine the solvent-induced effects on molecular properties.[23−25] Orientationally averaged local field factors can be used in calculating the dielectric constant and refractive index of different materials.[26] In electrical breakdown of insulating liquids,[27] finding points where the local field is very high, i.e., hot-spots, is useful. At hot-spots, an electron avalanche may be initiated that can lead to a conductive plasma channel and an electrical breakdown. Because this is the focus of this work, we calculate the full second-rank tensor of the local field response and discuss the largest components in detail.

The response of the local field to the external electric field has been calculated at the Hartree−Fock level of theory in terms of the nuclear electric-shielding factor, which is the effective field seen by the nucleus as the response to an applied
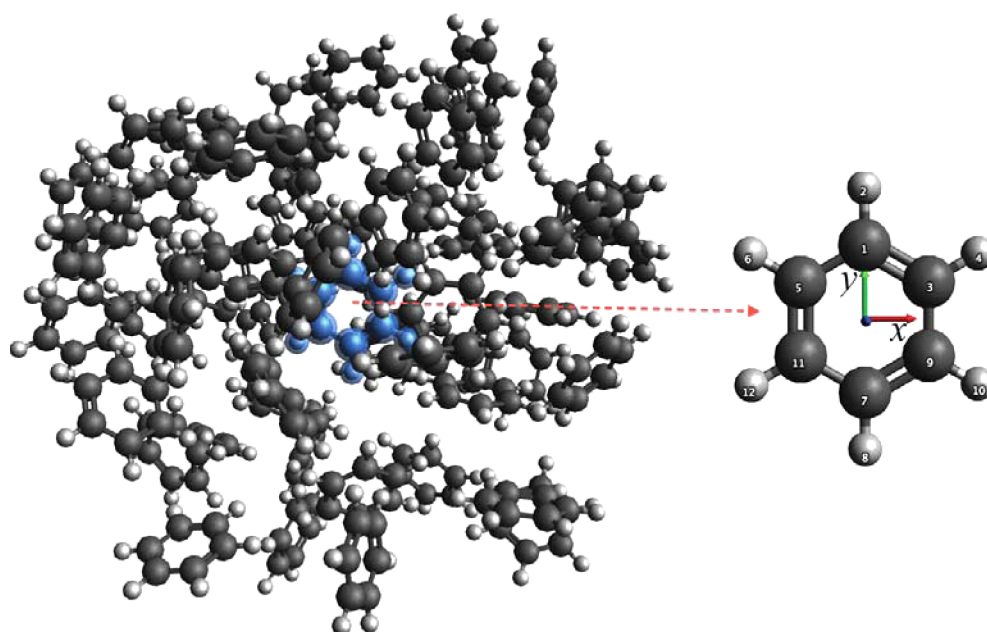
Figure 1. A typical cluster with the central benzene molecule marked in blue.

electric field.[28−30] Molecular dynamics (MD) simulations have also been used to calculate orientationally averaged local field factors essentially by extracting local field factors from simulations of the properties involved in electric-field-induced second-harmonic generation (EFISH) experiments.[31]

In our recent work on force-field models, a combined charge-transfer and point-dipole interaction (CT−PDI) model is extended to calculate the local field factor, and initial results were presented for the benzene and azobenzene dimers.[1] Here, we extend the study of local field factors to aggregates of molecules (in this case, liquid benzene due to its application in breakdown experiments).[32,33] The CT−PDI model[34−36] is basically a model to calculate the static and frequency-dependent polarizabilities, where the polarizability is partitioned into charge-transfer and dipole terms. In the CT−PDI model, these terms are obtained using the electronegativity equalization model (EEM)[10,37,38] rephrased in terms of the atom−atom charge-transfer (AACT) model[39] in combination with the PDI model.[2−6]

The CT−PDI model has several important features: (i) Atomic charges are replaced by charge-transfer terms using the AACT model, $q_I = \sum_K^N q_{IK}$.[39] (ii) A Gaussian charge distribution is used for each atom instead of point charges.[7] (iii) The model can be used for both metallic and nonmetallic systems, i.e., polarizabilities scale correctly with the size of the system.[34] In a metallic model such as EEM, the charge-transfer between two atoms at infinite distance is not zero. In the CT−PDI model, an energy cost for charge-transfer between atoms is added such that the charge-transfer is zero between atoms at infinite separation.[34,35] (iv) The partitioning of the polarizability into charge and dipole terms is advantageous because for different types of molecules, the main contribution will vary. For example, in azo dyes, the contribution of the dipole term to the polarizability at the absorption frequency is more significant than the charge term.[36] Also, the charge and the dipole term may add up to give a relatively large local field factor, or the two terms may to a large extent cancel each other.[1]

In our work, we are interested in the response of the optical properties to the frequency-dependent external field at the absorption frequency. Because these frequencies are in the UV−vis part of the spectrum, only the electronic degrees of freedom couple with the external field; i.e., only the electronic polarization contributes. MD simulations are carried out to generate liquid benzene configurations to be used as input for the calculation of the local field factors by means of the CT−PDI model. The local field factors, independent of the amplitude of the external field, are presented for liquid benzene at zero and the absorption frequency, and the linear susceptibility at the absorption frequency is determined by an approach similar to the Clausius−Mossotti method.[26] The excitation energy of a benzene molecule in liquid benzene is also calculated by the CT−PDI model.

■ COMPUTATIONAL DETAILS

The linear response of the charge-transfer and the dipole terms to a homogeneous frequency-dependent external electric field, $E_{I,\alpha}^{\text{ext}}(\omega) = E_\alpha^{\text{ext}}(\omega)$, is determined by finding the derivative of eq 1 with respect to $E_\alpha^{\text{ext}}(\omega)$ and solving the Lagrangian involving potential energies and kinetic energies of the atomic charge-transfer terms and the atomic dipole moments oscillating with the same frequency as the external electric field.[35,40] The details of the model can be found in ref 35.

The parameters of the CT−PDI model are optimized by fitting the full tensor of the complex frequency-dependent polarizabilities against time-dependent density functional theory (TDDFT)[41−43] polarizabilities through the first absorption maximum adopting finite life-times of the excited state.[44,45] The parameters are not reoptimized in this work, but the values reported previously for a series of hydrocarbon and azo molecules are adopted here.[1]

The molecular-dynamics (MD) simulations are performed using the LAMMPS package (June 28, 2014 version)[46] to generate sample configurations as shown in Figure 1. A system of 216 benzene molecules is generated in a cubic box with a length of 31.8 Å and periodic boundary conditions. The cutoff distance for van der Waals interactions is 15 Å, and the force-
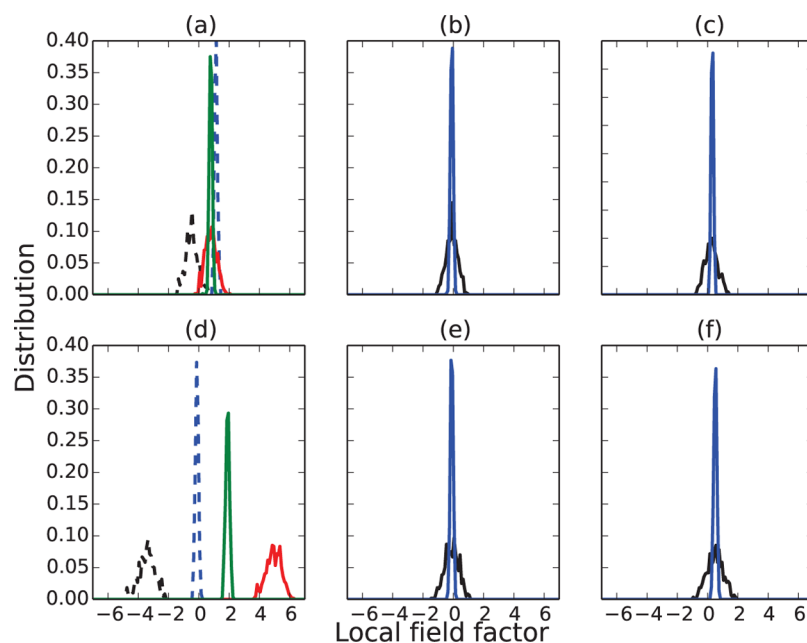
Figure 2. Local field factor distribution of the carbon (a, b, and c) and hydrogen (d, e, and f) atoms, respectively. The dashed line in (a) and (d) is $\frac{\partial E_{I,x}^{loc}}{\partial E_x^{ext}}$, and the solid line is $\frac{\partial E_{I,y}^{loc}}{\partial E_y^{ext}}$. Shown in (b) and (e) is $\frac{\partial E_{I,x}^{loc}}{\partial E_y^{ext}}$, and (c) and (f) are $\frac{\partial E_{I,z}^{loc}}{\partial E_z^{ext}}$. The blue and green lines are at zero frequency, and the black and red lines are at the absorption frequency, respectively.

field model used is OPLS-AA.[47−49] The system is equilibrated for 500 ps with a time step of 1 fs, and trajectories are generated in the canonical (NVT) ensemble at 300 K employing the Nosé−Hoover thermostat.[50,51] The simulation results are in good agreement with those in ref 49. The radial distribution functions (RDFs) are collected over 1500 ps, and the carbon RDF shows a small peak at around 4.3 Å and two large peaks at around 5.3 and 6.2 Å that are in good agreement with experimental data.[52] Snapshots of structures are taken every 2.5 ps, and clusters of 50 benzene molecules are chosen such that one benzene molecule is located at the center of the cluster, and the other molecules are rotated to be aligned to the axes of the moment of inertia of the central molecule. Subsequently, all tensor components of the local field factor are calculated. A total of 100 clusters are chosen, and the local field factor is calculated at carbon atom 1 and hydrogen atom 2 of the central molecule, marked in blue in Figure 1, giving 600 samples in total from the equivalence of carbon and hydrogen atoms in benzene.

The linear susceptibility is calculated using the CT−PDI model by combining molecular dynamic simulations and a modified Clausius−Mossotti equation,[26] where the PDI model is combined with the Clausius−Mossotti equation.[53] Here, the CT−PDI model is used instead of the PDI model, which gives an improvement by including the charge-transfer terms and the complex frequency dependence as compared to the PDI model, which includes only the static dipole term. Assuming the polarization in the Z-direction of the external field, the macroscopic polarization, P_Z, is given in terms of the molecular induced dipole moments,[26,54,55]

$$P_Z = N_d\langle\mu_\alpha\rangle_Z = N_d\langle\alpha_{\alpha\beta}^{mol}\rangle E_Z^{loc} \tag{3}$$

where N_d is the number density and $\langle\alpha_{\alpha\beta}^{mol}\rangle = \frac{1}{3}(\alpha_{xx} + \alpha_{yy} + \alpha_{zz})$ is the isotropic molecular polarizability. The linear susceptibility, $\chi_{ZZ}^{(1)}$ is defined as[26,54,55]

$$\chi_{ZZ}^{(1)} = \frac{\partial P_Z}{\partial E_Z^{ext}} = \frac{N_d\langle\alpha_{\alpha\beta}^{mol}\rangle}{1 - \frac{4\pi}{3}N_d\langle\alpha_{\alpha\beta}^{mol}\rangle} \tag{4}$$

The dielectric constant, ϵ, is obtained as[26,54,55]

$$\epsilon = 1 + 4\pi\chi_{ZZ}^{(1)} \tag{5}$$

The refractive index is thereby calculated from the square root of the dielectric constant.[26] As shown elsewhere, the Clausius−Mossotti relation can be improved by replacing the gas-phase value of $\langle\alpha_{\alpha\beta}^{mol}\rangle$ by the value obtained for a molecule in a cluster using a classical force-field model,[53] which is the model used here, using the CT−PDI model for the cluster.

The local field factor in a homogeneous external field is determined by

$$\frac{\partial E_{I,\alpha}^{loc}}{\partial E_\gamma^{ext}} = \delta_{\alpha\gamma} + \sum_{J\neq I}^{N}\left(\frac{-R_{IJ,\alpha}}{\tilde{R}_{IJ}^3}\frac{\partial q_J}{\partial E_\gamma^{ext}} \right.$$
$$\left. + \frac{3R_{IJ,\alpha}R_{IJ,\beta} - \delta_{\alpha\beta}\tilde{R}_{IJ}^2}{\tilde{R}_{IJ}^5}\frac{\partial\mu_{J,\beta}}{\partial E_\gamma^{ext}} \right) \tag{6}$$

The contribution of the macroscopic medium to the local field factor is calculated by the term $\frac{4\pi}{3}\chi_{ZZ}^{(1)}$ in the Lorentz approach,[56] which is an orientationally averaged contribution to the local field factor and can therefore not be directly added to eq 6.

RESULTS AND DISCUSSION

Figure 2 shows the local field factor distribution of the carbon and hydrogen atoms in the static limit and at the absorption frequency around 0.22 a.u. (6.0 eV). The local field factors are presented using eq 6, and the contribution from the linear susceptibility is discussed separately in Table 1. Only four

Table 1. $\frac{4\pi}{3}\chi_{ZZ}^{(1)}$ **for Benzene Clusters with Size** n **at Zero and the Absorption Frequency (a.u.)**

	n				
freq	10	20	30	40	50
0.0	0.426	0.441	0.424	0.424	0.424
0.22	1.778	1.773	1.767	1.767	1.767

components $(\partial E_{I,x}^{loc}/\partial E_x^{ext},\ \partial E_{I,y}^{loc}/\partial E_y^{ext},\ \partial E_{I,x}^{loc}/\partial E_y^{ext},$ and $\partial E_{I,z}^{loc}/\partial E_z^{ext})$ are shown because the other components have distributions very similar to that of $\partial E_{I,x}^{loc}/\partial E_y^{ext}$. At zero frequency, the distributions are narrower than at the absorption frequency, and Figure 2a–c shows that the largest local field factors $(\partial E_{I,x}^{loc}/\partial E_x^{ext},\ \partial E_{I,y}^{loc}/\partial E_y^{ext},\ \partial E_{I,x}^{loc}/\partial E_y^{ext},$ and $\partial E_{I,z}^{loc}/\partial E_z^{ext})$ at the carbon atom are around 1.8, 1.2, 0.2, and 0.6, respectively, while those at the hydrogen atom are around 0.3, 2.4, 0.2, and 0.9, as shown in Figure 2d–f, respectively. Figure 2a–c shows that at the absorption frequency, the largest local field factors $(\partial E_{I,x}^{loc}/\partial E_x^{ext},\ \partial E_{I,y}^{loc}/\partial E_y^{ext},\ \partial E_{I,x}^{loc}/\partial E_y^{ext},$ and $\partial E_{I,z}^{loc}/\partial E_z^{ext})$ at the carbon atom are around −1.3, 2.1, 1.0, and 1.5, respectively, while at the hydrogen atom they are around −4.8, 6.4, 1.1, and 1.9, as shown in Figure 2d–f, respectively.

Because we are interested in large local field enhancements, we will focus on configurations with high local field factors rather than averages. From the distribution plots, we found that the largest local field factor at the absorption frequency is 6.4 at the hydrogen atom. The local field factor at the hydrogen atom for this configuration is shown in Figure 3 as a function of
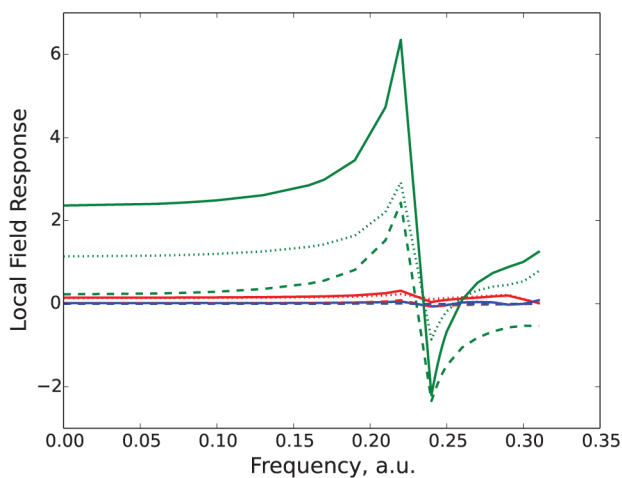

Figure 3. Largest local field response to the y-direction of the external electric field at the hydrogen atom in liquid benzene. The green line is $\frac{\partial E_{I,y}^{loc}}{\partial E_y^{ext}}$, and the red and blue lines are $\frac{\partial E_{I,x}^{loc}}{\partial E_y^{ext}}$ and $\frac{\partial E_{I,z}^{loc}}{\partial E_y^{ext}}$, respectively. The dashed line is the charge contribution, and the dotted line is the dipole contribution. (1 a.u. = 27.21 eV).

frequency. The local field factor, $\partial E_{I,y}^{loc}/\partial E_y^{ext}$, increases from 2.4 at zero frequency to 6.4 at the absorption frequency. The dipole contribution to the local field factor is larger than the charge term at frequencies below the absorption, although they are comparable at the absorption frequency, in line with our previous results.[1] The hydrogen RDF has three peaks located around 3.4, 4.6, and 6.7 Å, respectively. The intermolecular H−H distance in this configuration is around 2 Å, which results in a large local field factor because the local field factor depends strongly on the intermolecular distances.[1]

To investigate the dependence on the size of the benzene configuration, we calculated the local field factors at the carbon atom 1 and hydrogen atom 2 (see Figure 1 for labels) of the configuration, with the largest local field factor at 0 and the absorption frequency. The configuration is divided into smaller parts (clusters) where the number of molecules surrounding the central molecule is increased from $n = 2$ to 50. The results are presented in Table S1. Increasing the number of molecules leads to small changes in the local field factors. The number of molecules are a function of R scales by the volume R^3, whereas, e.g., the dipole−dipole interactions scale by R^{-3}, where R is the distance between molecules. At large distances, the individual intermolecular interactions become less important, and the effect of the surrounding molecules can be determined by the macroscopic polarization as discussed below. Table S1 shows that the local field factors at zero frequency converge more rapidly than at the absorption frequency.

In Figure 4a,b, the average of $\partial E_{I,y}^{loc}/\partial E_y^{ext}$ and its variance at the hydrogen atom are shown as a function of the number of
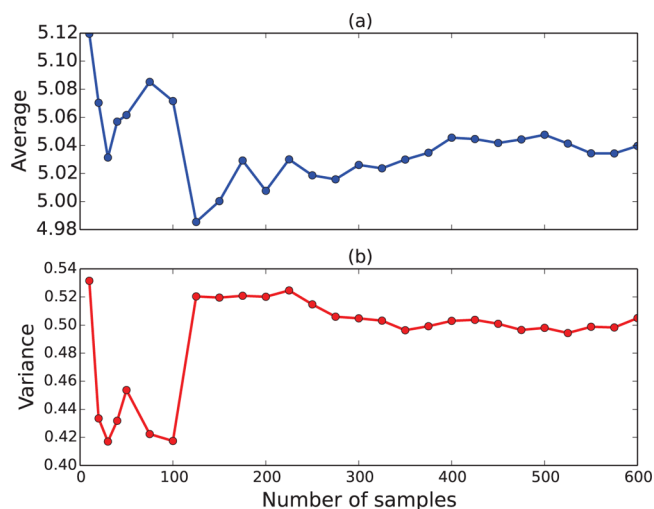

Figure 4. Average (a) and variance (b) of the local field factor, $\frac{\partial E_{I,y}^{loc}}{\partial E_y^{ext}}$, at the hydrogen atom at the absorption frequency as a function of the number of samples.

samples, respectively. Both quantities achieve reasonable convergence after 100 samples, indicating that the chosen number of samples is sufficient for the local field factor calculations. The convergence of the other components of the local field factor is also obtained after around 100 samples and is therefore not shown.

Figure 5a shows the distribution of the linear susceptibility at zero and the absorption frequency, respectively, and Figure 5b shows the dielectric constant as a function of frequency. The linear susceptibility is distributed around 0.1 at zero frequency, while it is around 0.4 at the absorption frequency. The real part of the dielectric constant is 2.3 at zero frequency, in good agreement with the experimental value of 2.2,[57] and it increases to 6.3 at the absorption frequency. The calculated refractive index at zero frequency is 1.51, in reasonable agreement with a calculated value of 1.49.[58] In ref 57, the refractive index has also been obtained from the Lorenz−Lorentz equation,[55] giving a value of 1.48 compared to the experimental value of around 1.50.[59] The experimental values at the frequencies of 0.08 and 0.1 a.u. at 298.4 K are around 1.50 and 1.52, respectively,[60] in
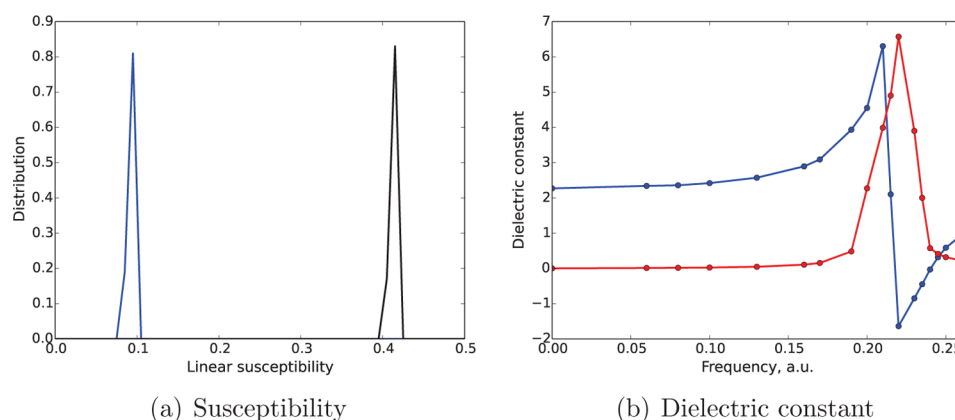
(a) Susceptibility

(b) Dielectric constant

Figure 5. (a) The susceptibility distribution of liquid benzene at zero (blue) and the absorption (black) frequencies. (b) The dielectric constant of liquid benzene. The real and imaginary parts are shown in blue and red, respectively.

reasonable agreement with the calculated ones at 300 K, around 1.53 and 1.55, respectively. The imaginary part of the dielectric constant is around 6.6 at the absorption frequency. From the imaginary part, one can find the dielectric loss of the liquid, which is an important factor in, for example, insulation applications in high-voltage devices.

The contribution of the linear susceptibility, $\frac{4\pi}{3}\chi_{ZZ}^{(1)}$, to the local field factor is presented in Table 1 for the cluster sizes from $n = 10$ to $n = 50$ at zero and the absorption frequency. For $n \geq 30$, the polarization response converges to the value 0.424 and 1.767 at 0 and the absorption frequency, respectively, indicating that the long-distance interactions can be replaced by a macroscopic polarization model.

It has been demonstrated that the CT−PDI model is capable of predicting the shift in excitation energies in good agreement with TDDFT for systems with different chain lengths (for example, alkanes and polyenes) and also for aromatic molecules and azo dyes with different substituents.[1,36] The $\pi \rightarrow \pi^*$ excitation energy of benzene in liquid phase is calculated to be around 6.0 eV, while it is around 6.3 eV in the gas phase. The experimental liquid-phase excitation energy is around 6.5 eV, while it is around 6.9 eV in the gas phase.[61] Thus, the CT−PDI shift in excitation energy when comparing the gas and liquid phases is in good agreement with the experimental shift.

CONCLUSIONS

To summarize, we have applied a model for the calculation of the local field factor that can be used for relatively large systems such as molecular clusters and macromolecules. For liquid benzene, the decomposition of the local field factor into charge and dipole terms indicates that the static local field is dominated by the dipole term, while at the absorption frequency, they contribute almost equally. At the carbon atom, the difference between the average local field factor at zero and the absorption frequency is around 0 for $\partial E_{I,y}^{loc}/\partial E_y^{ext}$, $\partial E_{I,x}^{loc}/\partial E_y^{ext}$, and $\partial E_{I,z}^{loc}/\partial E_z^{ext}$, respectively, while it is around 1.6 for $\partial E_{I,x}^{loc}/\partial E_x^{ext}$. At the hydrogen atom, the differences are around 3, 0, 0, and 3.3 for $\partial E_{I,y}^{loc}/\partial E_y^{ext}$, $\partial E_{I,x}^{loc}/\partial E_y^{ext}$, $\partial E_{I,z}^{loc}/\partial E_z^{ext}$, and $\partial E_{I,x}^{loc}/\partial E_x^{ext}$, respectively. The smaller difference at the carbon atom compared to the difference at the hydrogen atom is related to the cancellation of charge and dipole terms at the absorption frequency, which leads to a local field factor comparable to the static one. An advantage of a force-field model is the division into different contributions (in this case, a

charge and a dipole contribution). Therefore, we can classify the local field factors in two groups: either the charge and dipole terms add up to a substantial contribution, or they to a large extent cancel each other.

In addition to the local field factor, the model gives other static and optical properties at both the microscopic and the macroscopic scales such as the polarizability, susceptibility, dielectric constant, and absorption spectrum.

Developing the model further by including higher-order terms such as hyperpolarizabilities, nonlinear susceptibilities, and quadrupole moments can substantially improve the physics of the model and provide a useful tool for the calculation of numerous optical properties used in different applications.

ASSOCIATED CONTENT

Ⓢ Supporting Information
The Supporting Information is available free of charge on the ACS Publications website at DOI: 10.1021/acs.jpcb.5b07043.

Table showing the local field factor components of benzene clusters of increasing size. (PDF)

AUTHOR INFORMATION

Corresponding Author
*E-mail: per-olof.aastrand@ntnu.no.

Notes
The authors declare no competing financial interest.

REFERENCES

(1) Davari, N.; Haghdani, S.; Åstrand, P.-O.; Schatz, G. C. Local Electric Field Factors by a Combined Charge-Transfer and Point-Dipole Interaction Model. *RSC Adv.* **2015**, *5*, 31594−31605.
(2) Silberstein, L. Molecular Refractivity and Atomic Interaction. *Philos. Mag.* **1917**, *33*, 92−128.
(3) Silberstein, L. Molecular Refractivity and Atomic Interaction. II. *Philos. Mag.* **1917**, *33*, 521−533.
(4) Applequist, J.; Carl, J. R.; Fung, K.-F. An Atom Dipole Interaction Model for Molecular Polarizability. Application to Polyatomic

Molecules and Determination of Atom Polarizabilities. *J. Am. Chem. Soc.* **1972**, *94*, 2952−2960.

(5) Applequist, J. An Atom Dipole Interaction Model for Molecular Optical Properties. *Acc. Chem. Res.* **1977**, *10*, 79−85.

(6) Bode, K. A.; Applequist, J. A New Optimization of Atomic Polarizabilities in Halomethanes, Aldehydes, Ketones, and Amides by way of the Atom Dipole Interaction Model. *J. Phys. Chem.* **1996**, *100*, 17820−17824.

(7) Jensen, L.; Åstrand, P.-O.; Osted, A.; Kongsted, J.; Mikkelsen, K. V. Polarizability of Molecular Clusters as Calculated by a Dipole Interaction Model. *J. Chem. Phys.* **2002**, *116*, 4001−4010.

(8) Bakowies, D.; Thiel, W. Hybrid Models for Combined Quantum Mechanical and Molecular Mechanical Approaches. *J. Phys. Chem.* **1996**, *100*, 10580−10594.

(9) Thole, B. T. Molecular Polarizabilities Calculated with a Modified Dipole Interaction. *Chem. Phys.* **1981**, *59*, 341−350.

(10) Rappé, A. K.; Goddard, W. A., III Charge Equilibration for Molecular Dynamics Simulations. *J. Phys. Chem.* **1991**, *95*, 3358−3363.

(11) van der Velde, G. A. *A Realistic Coloumb Potential. MD and MC on Water*, Berendsen, H. J. C. ed.; CECAM: France, 1972; 38−39.

(12) Metiu, H.; Das, P. The Electromagnetic Theory of Surface Enhanced Epectroscopy. *Annu. Rev. Phys. Chem.* **1984**, *35*, 507−536.

(13) Moskovits, M. Surface-Enhanced Spectroscopy. *Rev. Mod. Phys.* **1985**, *57*, 783−826.

(14) Kedziora, G. S.; Schatz, G. C. Calculating Dipole and Quadrupole Polarizabilities Relevant to Surface Enhanced Raman Spectroscopy. *Spectrochim. Acta, Part A* **1999**, *55*, 625−638.

(15) Futamata, M.; Maruyama, Y.; Ishikawa, M. Local Electric Field and Scattering Cross Section of Ag Nanoparticles under Surface Plasmon Resonance by Finite Difference Time Domain. *J. Phys. Chem. B* **2003**, *107*, 7607−7617.

(16) Zhang, J. Z. Biomedical applications of shape-controlled plasmonic nanostructures: A Case Study of Hollow Gold Nanospheres for Photothermal Ablation Therapy of Cancer. *J. Phys. Chem. Lett.* **2010**, *1*, 686−695.

(17) Rycenga, M.; Camargo, P. H. C.; Li, W.; Moran, C. H.; Xia, Y. Understanding the SERS Effects of Single Silver Nanoparticles and Their Dimers, One at a Time. *J. Phys. Chem. Lett.* **2010**, *1*, 696−703.

(18) Sarkar, S.; Pradhan, M.; Sinha, A. K.; Basu, M.; Pal, T. Chelate Effect in Surface Enhanced Raman Scattering with Transition Metal Nanoparticles. *J. Phys. Chem. Lett.* **2010**, *1*, 439−444.

(19) Guidez, E. B.; Aikens, C. M. Origin and TDDFT Benchmarking of the Plasmon Resonance in Acenes. *J. Phys. Chem. C* **2013**, *117*, 21466−21475.

(20) Johnson, A. E.; Myers, A. B. Solvent Effects in the Raman Spectra of the Triiodide Ion: Observation of Dynamic Symmetry Breaking and Solvent Degrees of Freedom. *J. Phys. Chem.* **1996**, *100*, 7778−7788.

(21) Shimada, R.; Hamaguchi, H. Molecular Near-Field Antenna Effect in Resonance Hyper-Raman Scattering: Intermolecular Vibronic Intensity Borrowing of Solvent From Solute through Dipole-Dipole and Dipole-Quadrupole Interactions. *J. Chem. Phys.* **2014**, *140*, 204506.

(22) Shimada, R.; Kano, H.; Hamaguchi, H. Molecular Near-Field Effect and Intensity Enhancement of Solvent Modes in Resonance Hyper-Raman Scattering. *J. Raman Spectrosc.* **2006**, *37*, 469−471.

(23) Orozco, M.; Luque, F. J. Theoretical Methods for the Description of the Solvent Effect in Biomolecular Systems. *Chem. Rev.* **2000**, *100*, 4187−4225.

(24) Mennucci, B.; Cappelli, C.; Cammi, R.; Tomasi, J. Modeling Solvent Effects on Chiroptical Properties. *Chirality* **2011**, *23*, 717−729.

(25) Egidi, F.; Giovannini, T.; Piccardo, M.; Bloino, J.; Cappelli, C.; Barone, V. Stereoelectronic, Vibrational, and Environmental Contributions to Polarizabilities of Large Molecular Systems: A Feasible Anharmonic Protocol. *J. Chem. Theory Comput.* **2014**, *10*, 2456−2464.

(26) Jackson, J. D. *Classical Electrodynamics*, 2nd ed.; John Wiley and Sons: New York, 1975.

(27) Devins, J. C.; Rzad, S. J.; Schwabe, R. J. Breakdown and Prebreakdown Phenomena in Liquids. *J. Appl. Phys.* **1981**, *52*, 4531−4545.

(28) Lazzeretti, P.; Zanasi, R. Calculations of Nuclear Electric Shielding in Molecules. *Chem. Phys. Lett.* **1980**, *71*, 529−533.

(29) Lazzeretti, P.; Zanasi, R. Theory of Nuclear Electric Shielding in Molecules. *Phys. Rev. A: At., Mol., Opt. Phys.* **1981**, *24*, 1696−1704.

(30) Soncini, A.; Lazzeretti, P.; Bakken, V.; Helgaker, T. Calculation of Electric Dipole Hypershieldings at the Nuclei in the Hellmann-Feynman Approximation. *J. Chem. Phys.* **2004**, *120*, 3142−3151.

(31) Tu, Y.; Luo, Y.; Ågren, H. Molecular Dynamics Simulations Applied to Electric Field Induced Second Harmonic Generation in Dipolar Chromophore Solutions. *J. Phys. Chem. B* **2006**, *110*, 8971−8977.

(32) Yamashita, H.; Amano, H. Prebreakdown Phenomena in Hydrocarbon Liquids. *IEEE Trans. Electr. Insul.* **1988**, *23*, 739−750.

(33) Tortai, J. H.; Bonifaci, N.; Denat, A. Back to Results Insulating Properties of some Liquids after an Electrical Arc. *IEEE Trans. Dielectr. Electr. Insul.* **2002**, *9*, 3−9.

(34) Smalø, H. S.; Åstrand, P.-O.; Jensen, L. Nonmetallic Electronegativity Equalization and Point-Dipole Interaction Model Including Exchange Interactions for Molecular Dipole Moments and Polarizabilities. *J. Chem. Phys.* **2009**, *131*, 044101.

(35) Smalø, H. S.; Åstrand, P.-O.; Mayer, A. Combined Nonmetallic Electronegativy Equalization and Point-Dipole Interaction Model for the Frequency-Dependent Polarizability. *Mol. Phys.* **2013**, *111*, 1470−1481.

(36) Haghdani, S.; Davari, N.; Sandnes, R.; Åstrand, P.-O. Complex Frequency-Dependent Polarizability through the $\pi \rightarrow \pi^*$ Excitation Energy of Azobenzene Molecules by a Combined Charge-Transfer and Point-Dipole Interaction Model. *J. Phys. Chem. A* **2014**, *118*, 11282−11292.

(37) Mortier, W. J.; van Genechten, K.; Gasteiger, J. Electronegativity Equalization: Applications and Parametrization. *J. Am. Chem. Soc.* **1985**, *107*, 829−835.

(38) Stern, H. A.; Kaminski, G. A.; Banks, J. L.; Zhou, R.; Berne, B. J.; Friesner, R. A. Fluctuating Charge, Polarizable Dipole, and Combined Models: Parameterization from Ab Initio Quantum Chemistry. *J. Phys. Chem. B* **1999**, *103*, 4730−4737.

(39) Chelli, R.; Procacci, P.; Righini, R.; Califano, S. Electrical Response in Chemical Potential Equalization Schemes. *J. Chem. Phys.* **1999**, *111*, 8569−8575.

(40) Mayer, A.; Lambin, P.; Åstrand, P.-O. An Electrostatic Interaction Model for Frequency-Dependent Polarizability: Methodology and Applications to Hydrocarbons and Fullerenes. *Nanotechnology* **2008**, *19*, 025203.

(41) Runge, E.; Gross, E. K. U. Density-Functional Theory for Time-Dependent Systems. *Phys. Rev. Lett.* **1984**, *52*, 997−1000.

(42) Gross, E. K. U.; Dobson, J. F.; Petersilka, M. Density Functional Theory of Time-Dependent Phenomena. *Top. Curr. Chem.* **1996**, *181*, 81−172.

(43) Marques, M. A. L.; Gross, E. K. U. Time-Dependent Density Functional Theory. *Annu. Rev. Phys. Chem.* **2004**, *55*, 427−455.

(44) Norman, P.; Bishop, D. M.; Jensen, H. J. Aa.; Oddershede, J. Near-Resonant Absorption in the Time-Dependent Self-Consistent Field and Multiconfigurational Self-Consistent Field Approximations. *J. Chem. Phys.* **2001**, *115*, 10323−10334.

(45) Jensen, L.; Autschbach, J.; Schatz, G. C. Finite Lifetime Effects on the Polarizability within Time-Dependent Density-Functional Theory. *J. Chem. Phys.* **2005**, *122*, 224115.

(46) Plimpton, S. Fast Parallel Algorithms for Short-Range Molecular Dynamics. *J. Comput. Phys.* **1995**, *117*, 1−19.

(47) Jorgensen, W. L.; Tirado-Rives, J. The OPLS Potential Functions for Proteins. Energy Minimizations for Crystals of Cyclic Peptides and Crambin. *J. Am. Chem. Soc.* **1988**, *110*, 1657−1666.

(48) Jorgensen, W. L.; Severance, D. L. Aromatic-Aromatic Interactions: Free Energy Profiles for the Benzene Dimer in Water, Chloroform, and Liquid Benzene. *J. Am. Chem. Soc.* **1990**, *112*, 4768−4774.

(49) Fu, C.-F.; Tian, S. X. A Comparative Study for Molecular Dynamic Simulations of Liquid Benzene. *J. Chem. Theory Comput.* **2011**, *7*, 2240−2252.

(50) Nosé, S. A. Molecular Dynamics Method for Simulations in the Canonical Ensemble. *Mol. Phys.* **1984**, *52*, 255−268.

(51) Hoover, W. G. Canonical Dynamics: Equilibrium Phase-Space Distributions. *Phys. Rev. A: At., Mol., Opt. Phys.* **1985**, *31*, 1695−1697.

(52) Narten, A. H. X-Ray Diffraction Pattern and Models of Liquid Benzene. *J. Chem. Phys.* **1977**, *67*, 2102.

(53) Jensen, L.; Åstrand, P.-O.; Mikkelsen, K. V. Microscopic and Macroscopic Polarization in C_{60} Fullerene Clusters as Calculated by an Electrostatic Interaction Model. *J. Phys. Chem. B* **2004**, *108*, 8226−8233.

(54) Boyd, R. W. *Nonlinear Opt.*; Academic Press: San Diego, CA, 1992.

(55) Böttcher, C. J. F. *Theory of Electric Polarization*, 2nd ed.; Elsevier: Amsterdam, Netherlands, 1973.

(56) Kittel, C. *Introduction to Solid State Physics*, 4th ed.; Wiley: New York, 1971.

(57) Mardolcar, U.; de Castro, C. A. N.; Santos, F. J. V. Dielectric Constant Measurements of Toluene and Benzene. *Fluid Phase Equilib.* **1992**, *79*, 255−264.

(58) Janssen, R. H. C.; Bomont, J.-M.; Theodorou, D. N.; Raptis, S.; Papadopoulos, M. G. Computer Simulation of the Linear and Nonlinear Optical Properties of Liquid Benzene: Its Local Fields, Refractive Index, and Second Nonlinear Susceptibility. *J. Chem. Phys.* **1999**, *110*, 6463−6474.

(59) Lide, D. R. *Handbook of Chemistry and Physics*, 84th ed.; CRC Press: Boca Raton, FL, 2004.

(60) Rubio, J. E. F.; Arsuaga, J. M.; Taravillo, M.; Baonza, V. G.; Cáceres, M. Refractive Index of Benzene and Methyl Derivatives: Temperature and Wavelength Dependencies. *Exp. Therm. Fluid Sci.* **2004**, *28*, 887−891.

(61) Inagaki, T. Absorption Spectra of Pure Liquid Benzene in the Ultraviolet Region. *J. Chem. Phys.* **1972**, *57*, 2526−2530.